Research Square

Preprints are preliminary reports that have not undergone peer review.
They should not be considered conclusive, used to inform clinical practice,
or referenced by the media as validated information.

# Design of Silicene Nanopore Sensors for DNASequencing Application: Machine learning assisted DFT+NEGF Study

**Ashutosh shah**
Indian Institute of Technology Mandi
**Abhishek Sharma**
Indian Institute of Technology Mandi
**Arti Kashyap**
arti@iitmandi.ac.in

Indian Institute of Technology Mandi

**Research Article**

**Keywords:** Density Functional Theory, DNA sequencing, electronic transport, silicene nanoribbon, nanopore, quantum transport, supervised machine learning, classification, SHAP

**Posted Date:** January 27th, 2026

**DOI:** https://doi.org/10.21203/rs.3.rs-8673181/v1

**License:** This work is licensed under a Creative Commons Attribution 4.0 International License.
Read Full License

**Additional Declarations:** No competing interests reported.

# Design of Silicene Nanopore Sensors for DNA Sequencing Application: Machine learning assisted DFT+NEGF Study

Ashutosh Shah
*PhD Scholar (SCEE)*
*IIT Mandi*
Himachal Pradesh, India
D20052@students.iitmandi.ac.in

Abhishek Sharma
*SCEE*
*IIT Mandi*
Himachal Pradesh, India
abhi@iitmandi.ac.in

Arti Kashyap
*Professor (SPS)*
*IIT Mandi*
Himachal Pradesh, India
arti@iitmandi.ac.in

***Abstract*—Decoding the genetic code with electronic sensors requires devices that combine high signal fidelity with intelligent data interpretation. In this work, we present a first-principles quantum transport investigation of a Z-shaped silicene nanoribbon field-effect transistor (FET) incorporating a nanopore for single-nucleobase detection. The electronic structure and current–voltage characteristics are computed using density functional theory combined with the nonequilibrium Green's function formalism. The proposed Z-shaped architecture produces enhanced current levels, which are highly advantageous for achieving an improved signal-to-noise ratio in nanoscale sensing. Asymmetric electrode passivation yields substantially higher current discrimination among DNA bases than the symmetric all-hydrogen-passivated device. To enable reliable and automated base identification from the transport responses, a machine-learning-assisted framework is employed, where a Random Forest classifier attains 99.2% classification accuracy. SHAP analysis is used to interpret the model and identify the dominant physical descriptors governing nucleobase discrimination. The combined device–algorithm co-design establishes this platform as a high-sensitivity, label-free, and resource-efficient approach for next-generation electronic DNA sequencing.**

Index Terms- Density Functional Theory, DNA sequencing, electronic transport, silicene nanoribbon, nanopore, quantum transport, supervised machine learning, classification, SHAP.

**1. Introduction-** The use of Density Functional Theory (DFT) in combination with the nonequilibrium Green's function (NEGF) approach to design nanosensors for DNA sequencing is a challenging, complex and interdisciplinary problem. It demands not only a solid understanding of DFT and quantum transport theory but also a deep familiarity with state-of-the-art DNA sequencing technologies. Given the multifaceted nature of this problem, the article is introduced in two parts:

**1.1. Versatility of DFT:** DFT has firmly established itself as one of modern computational science's most powerful and broadly applicable tools. Rooted in first principles, DFT provides an accurate and scalable framework for predicting the ground-state properties of atoms, molecules, and condensed matter systems [1], [2]. Over the past two decades, its scope has expanded well beyond traditional materials modelling to encompass a broad spectrum of emerging fields, ranging from nanotechnology, quantum transport, and catalysis, to biophysics, forensic science, and biosensing [3], [4]. In particular, the integration of DFT with the NEGF formalism has enabled detailed studies of quantum transport in open systems, where the interplay between atomic structure and electron dynamics plays a crucial role [5]–[7]. This DFT+NEGF approach is now central to the understanding and designing nanoscale devices, molecular junctions, and increasingly, bioelectronic interfaces [8].

Such versatility stems from DFT's ability to offer atomistic resolution, quantitative electronic structure, and material-specific transport predictions under operational conditions. These capabilities are proving transformative in areas such as electrochemical sensing, where surface reactivity governs selectivity [9]; molecular recognition, where weak interactions define functionality [8]; and even DNA sequencing, where base-dependent conductance and charge transfer processes are key to signal differentiation [10], [11]. As experimental techniques push toward atomic-scale precision, the predictive insights offered by DFT-based modelling, especially when coupled with transport theories like NEGF, are complementary and often essential for interpreting measurements and guiding the design of next-generation technologies across disciplines.

**1.2. DNA Sequencing:** DNA sequencing is a transformative tool that has significantly advanced our understanding of genetics and molecular biology. By determining the precise order of nucleotides in a DNA molecule, researchers can gain valuable insights into gene functionality, genetic diversity, and the molecular basis of diseases [12]. Over the years, advancements in DNA sequencing technologies have drastically improved their speed, accuracy, and affordability. Nonetheless, existing methods still face many challenges related to sensitivity and precision [13]. Sanger sequencing, introduced in the late 1970s, was the first reliable method for determining DNA sequences. This technique employs chain termination to generate DNA fragments of varying lengths,

which are then separated by size to reconstruct the sequence [14]. While renowned for its accuracy and reliability, Sanger sequencing is labour-intensive, expensive, and unsuitable for large-scale applications like whole-genome sequencing due to its low throughput and short-read limitations [15]. Next-generation sequencing (NGS) has revolutionized the field by enabling the simultaneous sequencing of millions of DNA fragments. Technologies such as Illumina's sequencing-by-synthesis provide significantly higher throughput than Sanger sequencing at reduced costs [16]. NGS has facilitated large-scale initiatives, including the Human Genome Project. However, it requires DNA amplification, which can introduce errors and biases, especially in repetitive or GC (guanine-thymine) rich regions. Additionally, the short reads generated by NGS necessitate computationally intensive processes to assemble longer sequences, which can sometimes compromise accuracy [17]. Third-generation sequencing (TGS), including methods like PacBio's SMRT sequencing and Oxford Nanopore Technologies, overcomes many of these limitations by offering long-read sequencing capabilities [18]. These techniques can directly sequence extensive stretches of DNA, revealing structural variations and epigenetic modifications that are challenging for NGS to resolve. Nanopore sequencing, a standout among TGS technologies, reads DNA as it passes through a biological or solid-state nanopore without requiring amplification or labelling [19]. This simplifies sample preparation, lowers costs, and enables real-time analysis. However, challenges remain, such as higher error rates and difficulty identifying bases in homopolymeric and complex regions [13]. In nanopore-based sequencing, as DNA passes through the pore, each nucleotide alters the ionic current in a unique way, allowing for sequence determination [20]. Nanopore-based sequencing is a high-throughput, label-free, and amplification-free technique with three main types of nanopores: biological, artificial, and hybrid. Biological nanopores, typically embedded in lipid bilayers or polymer membranes, were pioneered with $\alpha$-hemolysin protein [21]. Widely used biological nanopores include $\alpha$-hemolysin, mycobacterium smegmatis porin A (MspA), and Phi29 [22]. Despite their sensitivity and simplicity, biological nanopores have limitations like size constraints and reduced stability, which have driven interest in solid-state nanopores [23]. These nanopores, fabricated from materials like silicon carbide (SiC), silicon dioxide ($SiO_2$), and aluminium oxide ($Al_2O_3$), offer higher stability and customizable dimensions [24]. Hybrid nanopores merge the benefits of biological and solid-state nanopores, as demonstrated by early designs integrating $\alpha$-hemolysin into silicon nitride (SiN) films [25].

To address the limitations of conventional solid-state nanopores (SSNs), several advanced detection strategies have been explored, including optical sensing, tunnelling current measurements, and nanopore field-effect transistor (FET) detection. Unlike traditional ionic blockade methods, nanopore FET sensors provide several decisive advantages. They exhibit relatively high baseline currents in the microampere range, offering improved signal-to-noise ratios (SNR) and stable high-frequency responses, thereby supporting high-bandwidth operation beyond the reach of conventional SSNs. Moreover, their CMOS-compatible fabrication process supports seamless integration and multiplexing within a single analytical platform, eliminating the need for complex microfluidic architectures. Beyond silicon-based implementations, emerging two-dimensional (2D) materials such as graphene and $MoS_2$ have further expanded the potential of nanopore FET sensors, offering enhanced sensitivity, tunable surface chemistry, and superior electrical performance.

The choice of materials for constructing nanopore devices is critical. Graphene has emerged as a promising candidate due to its remarkable electrical and structural properties. With a thickness of 0.35 nm, comparable to the spacing between DNA bases, graphene is ideal for sequencing applications [26]. Functionalizing graphene membranes with materials such as gold nanoparticles further enhances their sensitivity and selectivity [27]. Graphene nanoribbons (GNRs), patterned into armchair (AGNR) or zigzag (ZGNR) geometries, provide additional tunability for electronic sensing. Solid-state nanopore sensors typically operate via tunnelling, field-effect sensing, or ionic current detection [28]. Owing to its atomic thickness, graphene is particularly effective for field-effect and ionic current based detection, where the translocation of negatively charged DNA through the nanopore modulates the device conductance and produces base-specific current signatures [29]. Beyond graphene, the rapidly expanding family of two-dimensional materials has opened new opportunities for next-generation biosensing platforms. In particular, silicon-based two-dimensional systems are attracting growing interest due to their intrinsic compatibility with existing semiconductor technology and their potential for seamless device integration. Among them, silicene the two-dimensional allotrope of silicon has been both theoretically predicted and experimentally demonstrated as a highly promising material for a wide range of nanoelectronic applications, including high-performance field-effect transistors, flexible electronics, and nanoscale sensing platforms [30]–[43]. Comprehensive experimental and theoretical investigations have established that, with appropriate growth and encapsulation strategies, silicene can be reliably integrated into functional electronic architectures, including high-performance FETs and bendable membranes [44] [45]–[51] . Owing to its intrinsic compatibility with the existing silicon-based technology infrastructure, silicene represents a natural bridge between emerging two-dimensional materials and conventional complementary metal–oxide–semiconductor (CMOS) electronics.

Building on this foundation, prior theoretical studies have specifically demonstrated the feasibility of silicene as a FET channel material [52]–[56] and as an effective electronic sensor for DNA nucleobases [57]. More recently, Bhai and Ganguly [58] provided direct experimental validation of the silicene–DNA interaction through infrared and Raman spectroscopic measurements, where distinct vibrational shifts were observed upon nucleobase adsorption. These experimental signatures were found to be in close agreement with first-

principles predictions, confirming that silicene can stably physisorb DNA nucleobases while exhibiting strong and selective electronic sensitivity [59]. Collectively, this experimental–theoretical convergence firmly establishes silicene as a robust and technologically attractive platform for next-generation DNA sensing devices.

Previous first-principles studies have demonstrated the feasibility of silicene-based nanopore devices for DNA sequencing using a conventional straight-channel geometry [60]. However, the reported current levels in such silicene nanopore FETs remain relatively low, typically in the nanoampere to sub-nanoampere regime, which limits the achievable signal-to-noise ratio and detection robustness.

In this work, we investigate nanopore-based sequencing sensors by integrating Z-shaped silicene nanoribbons, a geometry specifically designed to overcome these limitations by enhancing both the magnitude and the distinguishability of the electrical response. Furthermore, we introduce a machine-learning-assisted DNA base classification framework, enabling reliable and automated identification of nucleobases from the device transmisson signatures. The combined device-algorithm co-design significantly improves the sensitivity, selectivity, and practical applicability of silicene-based nanopore sequencing platforms.

## 2. Methodology

The simulations employ DFT combined with the NEGF formalism to model the sensor's electronic transport properties using Nanodcal software package [61]. This approach enables the calculation of transmission spectra and currents for various DNA bases. Before electronic transport measurements, the Z-shaped device and nucleobases were optimized using DFT until atomic forces were reduced to below 0.05 eV/Å. The exchange-correlation function was parameterised using the Perdew-Burke-Ernzerhof (PBE) method. The NEGF approach combined with DFT examined various electronic properties, including the transmission spectrum and current. To compute the charge density, an 120 Hartree mesh cut-off was applied. Brillouin zone integration used a **k**-point sampling of 1×1×100. The transverse current was derived from the transmission spectrum using NEGF. DNA base orientations were considered during translocation through the nanopore, as orientation impacts current and transmission spectra. The transmission probability at energy $E$ is then calculated as [62]. The transmission probability at energy $E$ is calculated using the Landauer–Büttiker formalism within the NEGF framework as

$$T(E) = \mathrm{Tr}[\Gamma_L(E)\, G^r(E)\, \Gamma_R(E)\, G^a(E)]\,, \qquad (1)$$

where $G^r(E)$ is the retarded Green's function of the device region and $G^a(E) = [G^r(E)]^\dagger$ is the corresponding advanced Green's function. The matrices $\Gamma_L(E)$ and $\Gamma_R(E)$ describe the coupling between the device and the left and right electrodes, respectively, and are given by

$$\Gamma_{L,R}(E) = i\left[\Sigma_{L,R}(E) - \Sigma^\dagger_{L,R}(E)\right], \qquad (2)$$

where $\Sigma_{L,R}(E)$ are the electrode self-energy matrices. The trace operator $\mathrm{Tr}[\cdots]$ represents the summation over all available quantum transport channels. Physically, $T(E)$ measures the probability that an electron with energy $E$ injected from the left electrode is transmitted through the device and collected by the right electrode, incorporating the effects of quantum coherence, contact coupling, and electronic structure of the system.

The current through the device is obtained using the Landauer–Büttiker formalism [63]:

$$I(V) = \frac{2e}{h}\int_{-\infty}^{+\infty} T(E,V)\left[f(E-\mu_L) - f(E-\mu_R)\right] dE \quad (3)$$

where $f(E)$ is the Fermi–Dirac distribution function, and $\mu_{L,R} = E_F \pm eV/2$ denotes the electrochemical potentials of the left and right electrodes under an applied bias voltage $(V)$.

**3. Results and Discussion -** The simulation workflow (Fig. 1) comprised multiple stages to evaluate the potential of a Z-shaped silicene nanoribbon field-effect transistor (FET) for DNA base detection. Initially, Density Functional Theory (DFT) calculations have been performed to study the physisorption of individual DNA nucleobases - adenine, guanine, cytosine, and thymine, on the surface of the silicene nanoribbon. This step provided critical insights into the interaction strength, preferred adsorption sites, and electronic modifications induced by the nucleobases. Key parameters such as effective potential profiles, and density of states (DOS) were analysed to understand the electronic fingerprints associated with each base. Following this, the DFT-NEGF based quantum transport simulations have been conducted to model the complete device. The base-specific adsorption configurations obtained from the structural analysis, is used as input to calculate the current-voltage (I–V) characteristics under small source drain bias. These simulations revealed how each nucleobase modulates the transmission spectrum and output current, demonstrating the sensor's capability for label-free, sequence-specific detection of DNA based on electronic response variation.

### 3.1 Analysis of the Suitability of Silicene for DNA sensing

We have carried out first-principles DFT calculations to investigate the fundamental electronic interactions that define the operation of silicene-based DNA sequencing devices. Our optimized geometries reveal two distinct adsorption regimes for DNA nucleobases on silicene. Guanine (G) and cytosine (C) approach the silicene surface much more closely, with equilibrium distances in the range of ∼1.8-2.0 Å, whereas adenine (A) and thymine (T) remain at significantly larger separations of ∼3.0-3.3 Å, characteristic of van der Waals contact distances (Fig. 2 and 3). As a result of this strong distance dependence, G and C form weak covalent (quasi-chemical) bonds with the underlying silicon atoms through Si-O interactions and are therefore classified as *weakly chemisorbed*, while

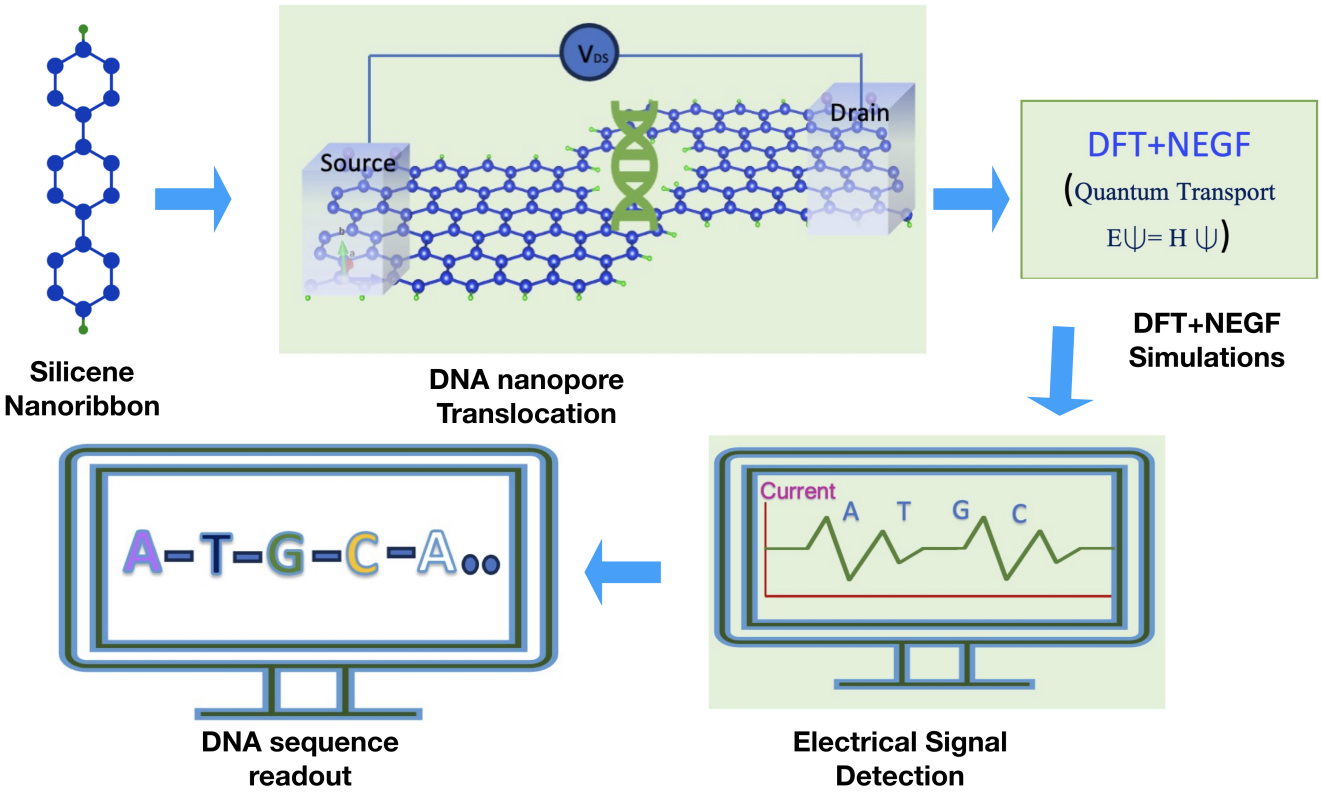



Fig. 1. Simplified DNA nanopore sequencing simulation framework

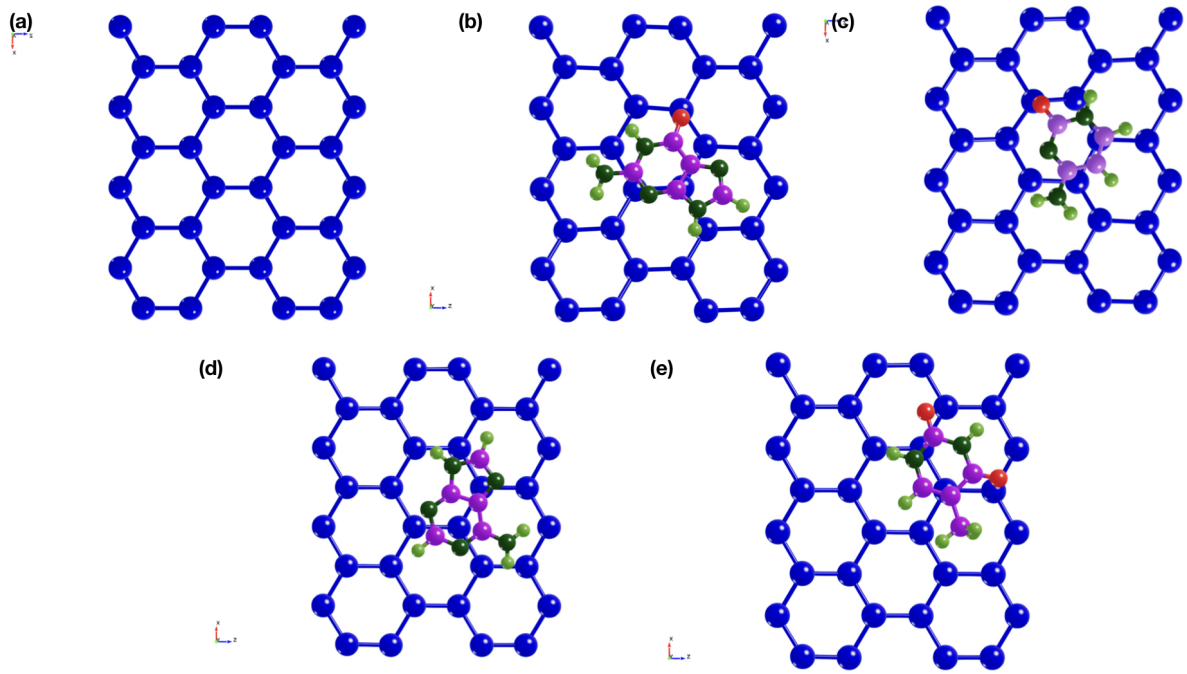



Fig. 2. DNA bases physiorbtion top view (a) pristine silicene (b) guanine on silicene (c) cytosine on silicene (d) adenine on silicene (e) thymine on silicene. light green-hydrogen, blue- silicene, red- oxygen, dark green- carbon, purple- nitrogen.

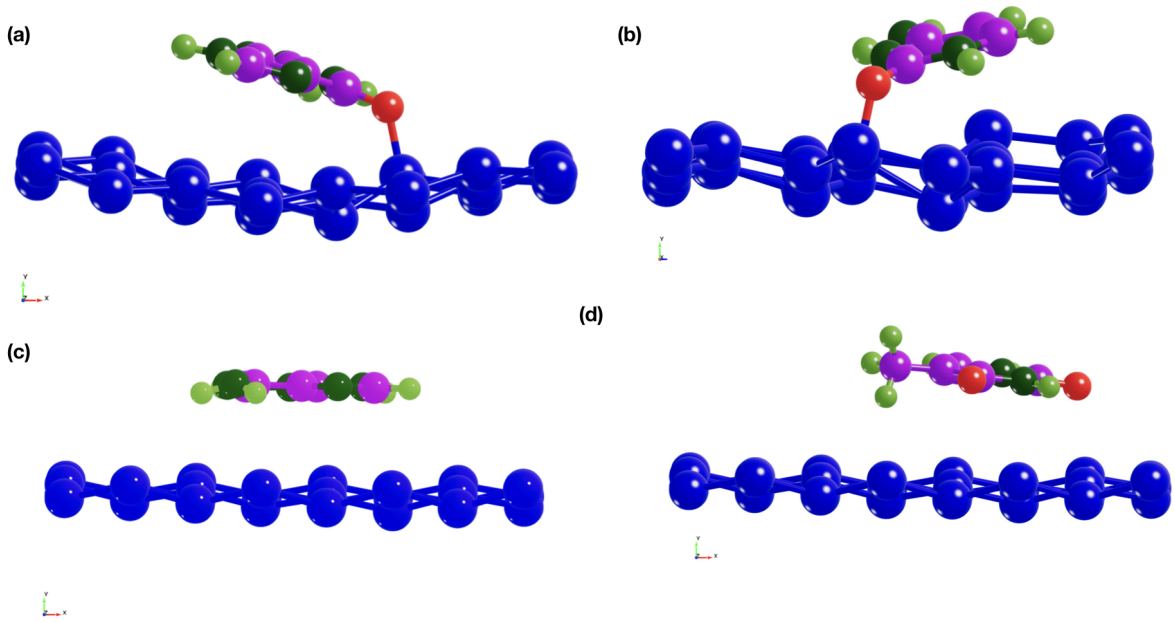



Fig. 3. DNA bases physiorbtion on silicene side view (a) guanine on silicene (b) cytosine on silicene (c) adenine on silicene (d) thymine on silicene. light green-hydrogen, blue- silicene, red- oxygen, dark green- carbon, purple- nitrogen

A and T interact purely through dispersive and electrostatic forces and remain *physisorbed*.

In addition, we observe a pronounced local structural distortion of the silicene sheet in the vicinity of guanine and cytosine adsorption. The silicon atoms beneath G and C are displaced downward, producing a shallow *bowl-like* deformation of the silicene lattice. This deformation originates from the stronger interfacial coupling and reduced Si-O bond length, and is absent for adenine and thymine where the interaction is much weaker. Such localized bending of the silicene surface under strongly interacting nucleobases has also been reported in earlier studies and our results closely reproduce this behavior, providing further validation of our computational findings [58], [59]. This coexistence of weak chemisorption and physisorption is highly beneficial for sensing applications, as it enables strong electronic sensitivity while preserving the intrinsic transport properties of silicene.

TABLE I
EQUILIBRIUM BOND LENGTH BETWEEN NUCLEOBASE AND SILICENE.

| Nucleobase | Closest Interaction | Bond Length (Å) |
|---|---|---|
| Adenine (A) | Si-H | ∼3.23 |
| Cytosine (C) | Si-O | ∼1.82 |
| Guanine (G) | Si-O | ∼1.89 |
| Thymine (T) | Si-H | ∼3.08 |

**3.1.1 Effective Potential Analysis** The effective electrostatic potential profiles of the silicene channel in the presence of the DNA nucleobases were analyzed using both one-dimensional line plots and three-dimensional isosurface visualizations. The line profiles extracted along the transport direction reveal pronounced, base-dependent potential wells whose depths and spatial extents differ for each nucleobase, reflecting distinct charge redistribution patterns induced by molecular physisorption. These quantitative variations are corroborated by the three-dimensional electrostatic potential isosurfaces, which provide a real-space representation of the Coulomb landscape at the molecule–silicene interface. As illustrated in Fig. 4 and 5, the adsorbed nucleobase produces a localized region of enhanced electrostatic potential (purple isosurfaces) directly above the silicene channel, confirming the formation of an interface dipole driven by intermolecular polarization. The confinement and intensity of these isosurfaces differ markedly among adenine, thymine, cytosine, and guanine, thereby establishing distinct electrostatic fingerprints for each base. This combined one-dimensional and three-dimensional electrostatic analysis demonstrates that although all bases interact via physisorption, their unique molecular charge distributions imprint characteristic modifications onto the channel potential, which subsequently govern the observed modulation of electronic transport in the silicene FET sensor.

**3.1.2 Analysis of Electronic Perturbation and Density of States (DOS)**

Our analysis of the density of states reveals that each nucleobase uniquely perturbs the electronic landscape of the silicene sheet (Fig. 6 (a)-(e)). Pristine silicene exhibits a semimetallic character, with a Dirac-like point near the Fermi level. However, upon nucleobase adsorption, localized states

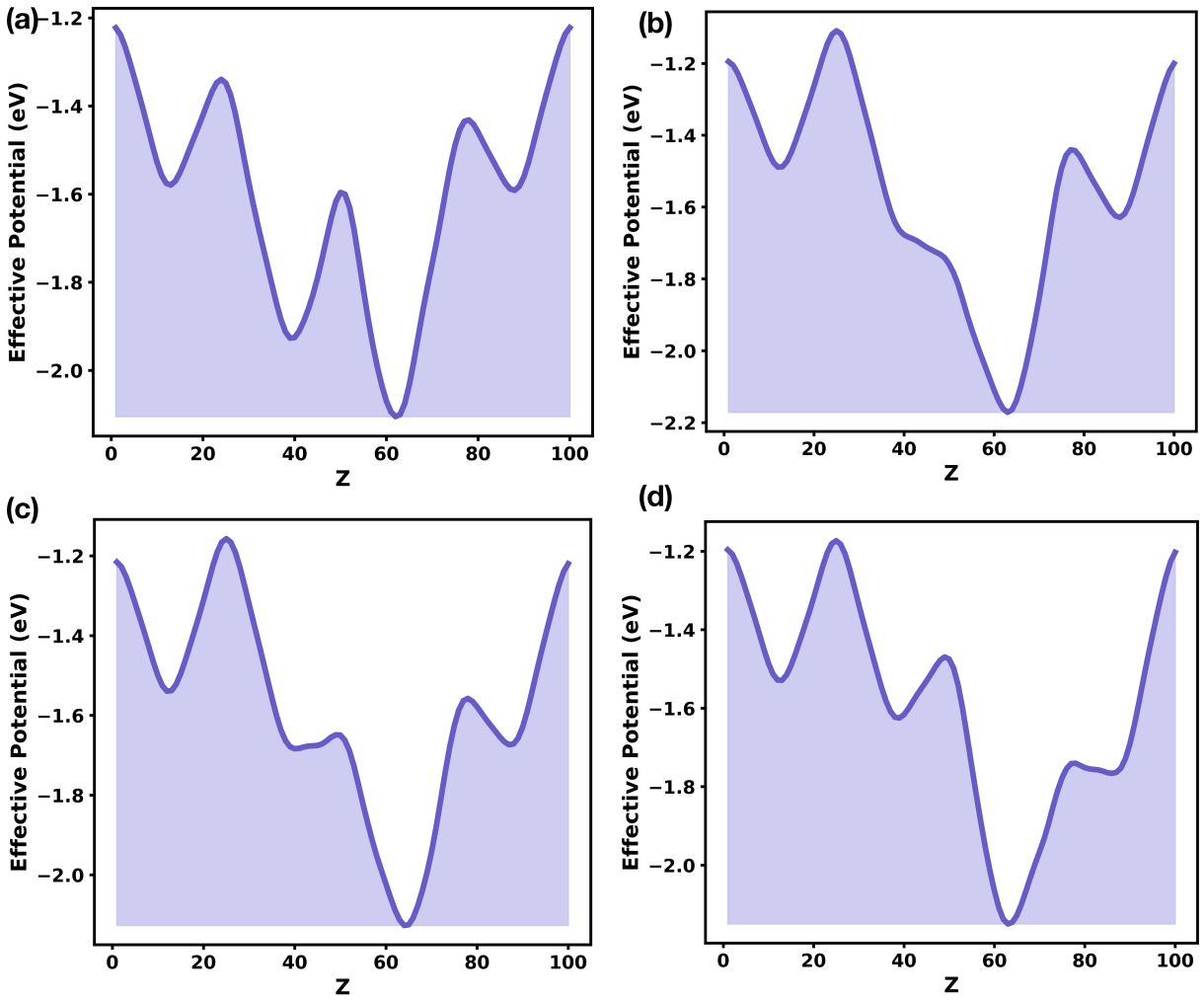



Fig. 4. Base-specific effective potential profiles of the silicene channel showing distinct electronic signatures induced by the physisorption of DNA nucleobases (a) guanine (b) cytosine (c) adenine (d) thymine

emerge in the vicinity of the Fermi level, disrupting the band symmetry and indicating charge redistribution at the interface. The energy position, intensity, and spread of these induced states vary with the nucleobase, reflecting the specific nature of their $\pi$-$\pi$ and van der Waals interactions with silicene.

Notably, cytosine and guanine cause more prominent shifts and spectral broadening near the Fermi level compared to adenine and guanine, owing to their higher binding energies as reported in earlier DFT studies [52]. Additionally, the DOS features associated with adenine and thymine exhibit partial charge delocalization into silicene, a potential marker for enhanced carrier modulation. This nucleobase specific DOS signature provides a strong foundation for electronic detection, as even subtle shifts in DOS can significantly alter the transport properties of silicene based devices.

Importantly, such differential orbital coupling can be exploited to define an electronic fingerprint for each nucleobase. This offers a quantum-level mechanism for selectivity in field-effect or tunnelling-based sensors, where variations in hybridization influence the charge injection barrier and local density of states at the contact. These findings reinforce the idea that silicene, due to its high surface reactivity, serves as a promising 2D platform for electronic biosensing applications targeting single-nucleotide resolution.

Building on the DFT-based insights, our study establishes the silicene nanosheet as a structurally and electronically suitable platform for DNA nucleobase sensing. The detailed analysis of binding energies, density of states, and frontier orbital hybridization confirms that each nucleobase perturbs the silicene sheet in a distinct and reproducible manner, creating unique electronic fingerprints. These electronic modifications, particularly the localized states near the Fermi level and nucleobase-specific hybridization patterns, form the theoretical foundation for charge transport modulation. While computationally efficient physisorption models are valuable for preliminary screening of material interactions, they cannot reliably predict the final conductance of a geometrically different device. To translate these findings into a realistic

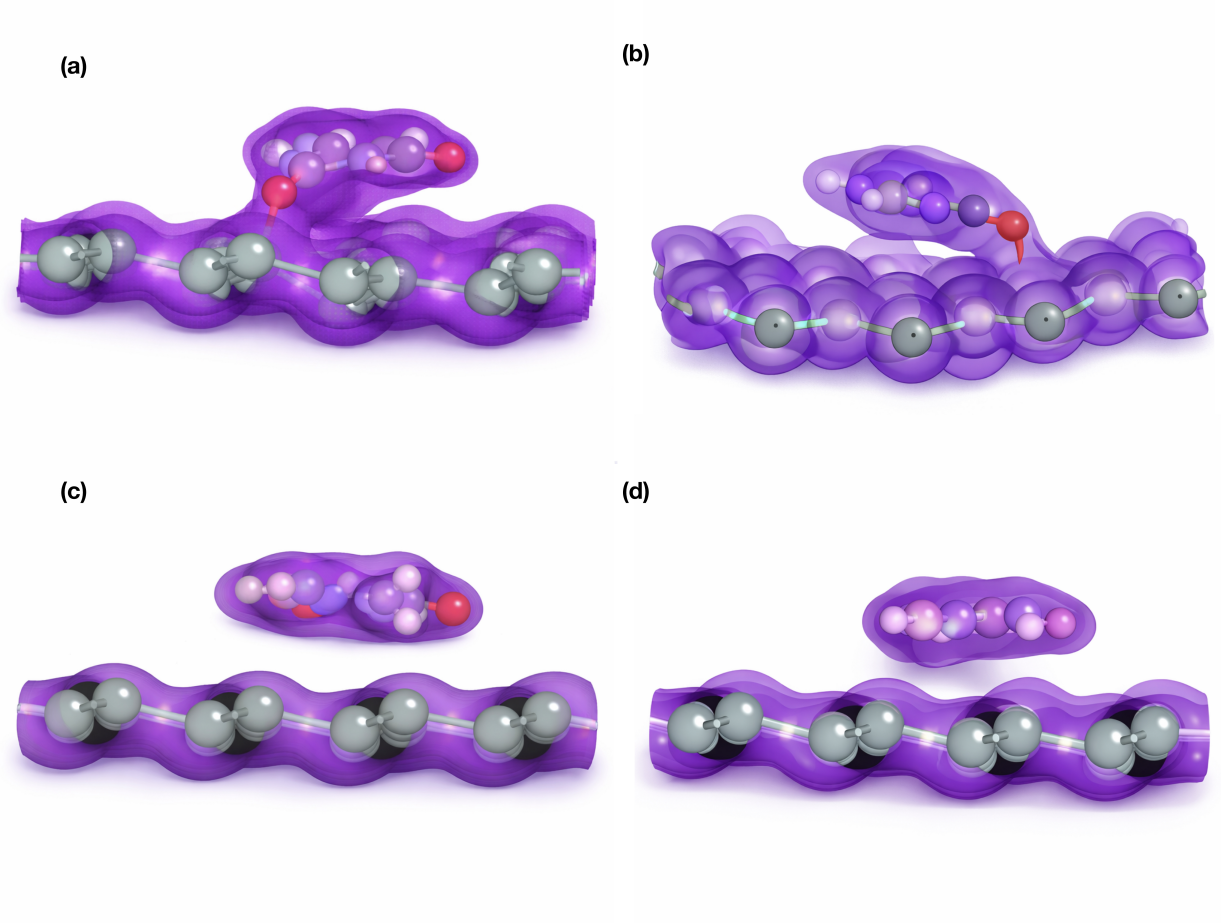



Fig. 5. Three-dimensional effective potential isosurface of the silicene channel with an adsorbed DNA nucleobase. The purple isosurfaces represent regions of enhanced electrostatic potential induced by molecular physisorption. The localized potential accumulation above the silicene surface confirms strong interfacial polarization and the formation of an interface dipole, which governs carrier transport in the device (a) guanine (b) cytosine (c) adenine (d) thymine

sensing scenario, we advance to quantum transport simulations using the NEGF formalism. Here, the Z-silicene channel is integrated between semi-infinite electrodes, with each nucleobase introduced in the sensing region. Remarkably, the calculated current–voltage (I–V) characteristics reveal clearly distinguishable transport signatures for all four nucleobases, reflecting the patterns of perturbations predicted by DFT. Thus, the DFT analysis serves not only as a fundamental step in understanding the base–silicene interaction but also as a critical input to guide and interpret device-level behavior. In the following section, we present and discuss the quantum transport results in detail, highlighting their correlation with the underlying electronic structure.

## 4. Nanopore-based DNA Sensor

### 4.1 DFT Study of Electrodes

Before designing the field-effect transistor (FET) for DNA sequencing, it is essential to carefully examine the nature of the electrodes, as their electronic structure significantly influences charge transport through the device. To this end, we performed DFT calculations on three different edge-passivated silicene nanoribbon electrodes, shown in Fig. 7(a)-(c). In the first configuration [Fig. 7(a)], both edges of the silicene ribbon are passivated with hydrogen atoms, representing a chemically stable and symmetric baseline system. In the second configuration [Fig. 7(b)], one edge is passivated with cobalt (Co) and the other with hydrogen, introducing structural asymmetry and additional metallic states. The third configuration [Fig. 7(c)] features cobalt atoms on both edges.

The corresponding electronic band structures are presented in Fig. 8(a)-(c). As seen in Fig. 8(a), the fully hydrogenated electrode shows a minimal number of electronic bands near the Fermi level, with only two bands contributing to conduction. This suggests limited availability of conducting channels, which could restrict current flow in the device. In contrast, the electrode with asymmetric Co-H passivation [Fig. 8(b)] exhibits a significant increase in the number of bands near the Fermi level. This enhancement arises from the presence of cobalt atoms, which introduce additional $d$-orbital states that hybridize with the silicene bands, thereby enriching the electronic spectrum. The fully cobalt-passivated electrode [Fig. 8(c)] also shows a similarly dense band structure, but with due to not having asymmetry, it is less favourable for controlled sensing.

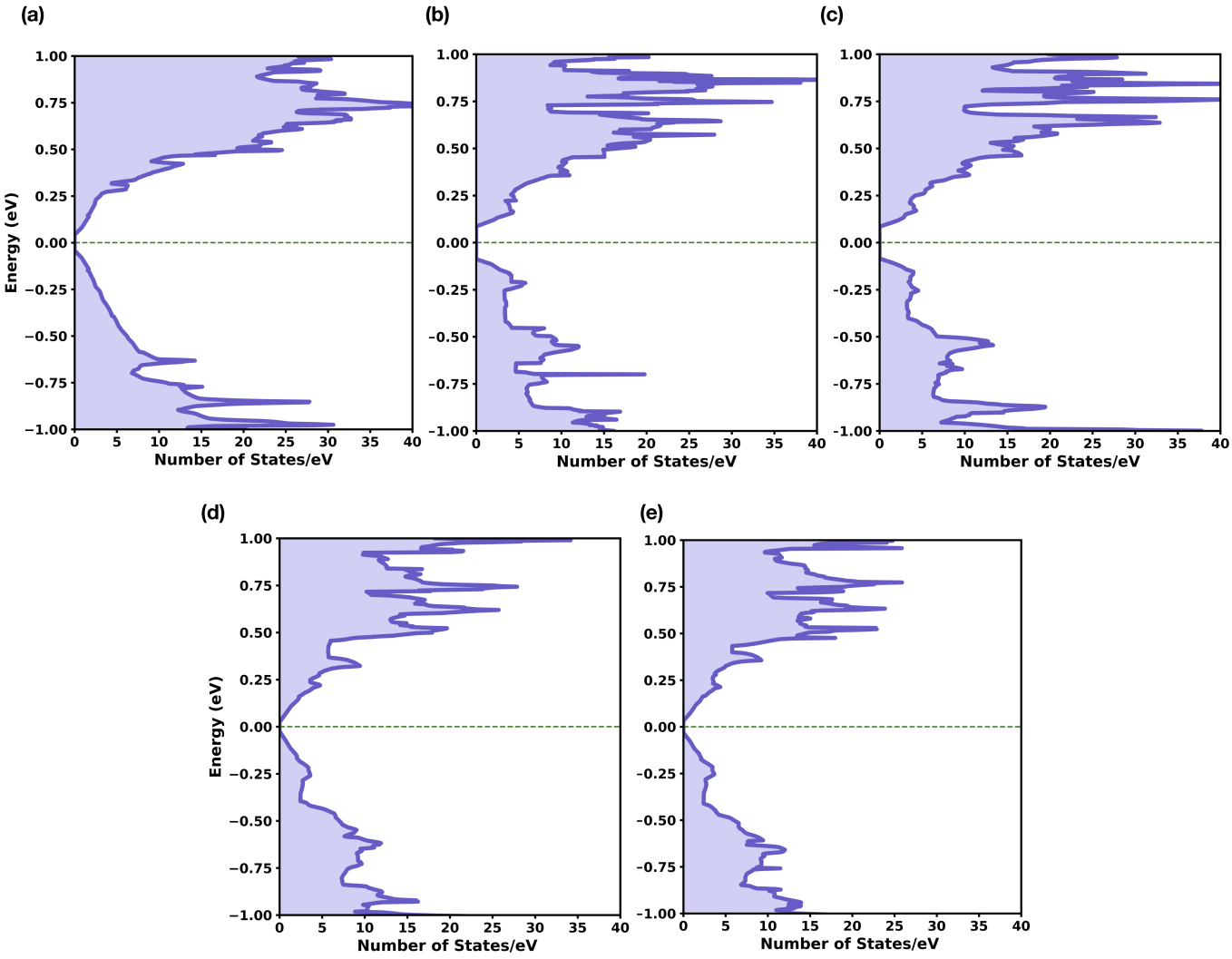



Fig. 6. Density of states (DOS) of (a) nanopore without bases (b) adenine (c) guanine (d) thymine (e) cytosine

Among these configurations, the asymmetric Co-H passivated electrode strikes an optimal balance between chemical simplicity and electronic richness. The increase in available states near the Fermi level is expected to improve sensitivity to external perturbations, such as nucleobase adsorption, by enabling greater modulation of charge transport. Therefore, this configuration is chosen for the source and drain electrodes in our DNA sensing FET device.

### 4.2 Geometry of Nanopore-based DNA Sensor

Fig. 9 illustrates the proposed DNA sequencing approach, which utilises a Z-shaped silicene nanoribbon. The Z-shaped FET incorporates a nanopore positioned centrally within its zigzag silicene channel. Zigzag silicene nanoribbons serving as source and drain terminals, the device integrates a gate terminal beneath the channel for enhanced modulation of electronic properties. The nanopore, sized at approximately 12 Å, allows for the translocation of single DNA strands, ensuring accurate detection of individual nucleobases. The Z-shaped configuration increases the sensor's sensitivity by enlarging the interaction surface with DNA molecules. To optimize performance, the sensor edges are passivated with hydrogen atoms. This design reduces noise and stabilizes the silicene structure, minimizing interactions between the DNA bases and the sensor. The absence of doping in the source, drain, and gate regions further ensures the preservation of silicene's intrinsic electronic properties, enhancing device reliability. The incorporation of cobalt atoms in source significantly influences the performance of the Z-shaped silicene sensor. These passivated cobalt atoms alter the local electronic structure of silicene, increasing its sensitivity to the electronic signatures of DNA bases. Cobalt atoms, in

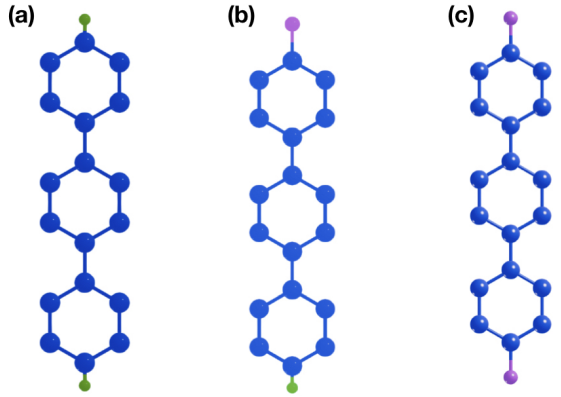



Fig. 7. Electrode selection of FET Sensor with different passivation (a) With all Hydrogen, (b) with one Co and another H (c) with both Co

particular, are favoured for their superior functionalization chemistry and lower contact resistance compared to other transition metal.

### 4.3 Transmission Spectrum

The analysis of the transmission spectrum provides crucial insights into the performance of the Z-shaped device for DNA base detection. Each nucleobase positioned within the nanopore produces a unique electrical response when analyzing the zero-bias transmission spectrum (Fig. 11 (a)-(d)). This distinction in transmission spectra offers promising potential for identifying individual DNA bases. Furthermore, comparing nanopores passivated with cobalt at the source and hydrogen passivation highlights the impact of edge functionalization on sensor behaviour. The Cobalt passivated configuration exhibits a higher number of transmission peaks around Fermi (as shown in Fig. 11 (c)). DNA bases fall into two categories: pyrimidine bases (cytosine and thymine) and purine bases (guanine and adenine). The major difference is their size. Transmission spectrum analysis shows that the purine and pyrimidine bases, with distinct chemical structures, influence the sensor's transport characteristics differently, allowing differentiation between the two groups under a fixed bias voltage. Purine bases have two carbon-nitrogen rings, while pyrimidines have one, resulting in higher currents for purines.

### 4.4 Transverse Current

The sensor's ability to distinguish DNA bases hinges on its capacity to measure variations in transverse current as the bases translocate through the nanopore. The transverse current is calculated by integrating the transmission spectra, with each base orientation and lateral position contributing a unique current interval. The results revealed that the sensor could reliably differentiate between the four nucleobases based on their distinct current ranges. The transverse current analysis further reveals the device's response to DNA bases. Each DNA base induces unique variations in transverse current when positioned in the nanopore. Cobalt passivation increases the transverse current rate compared to hydrogen passivation (Fig. 12), underscoring the importance of edge functionalization in enhancing sensor sensitivity and better differentiation among base signals (Fig. 13. Cobalt is suppressing current a bit, compared to a pure hydrogenated nanopore, but it gives much more differentiable base signals. Additionally, applying a dual gate configuration further boosts sensitivity, leading to higher transverse current rates [64]. This enhanced sensitivity shows promise for faster DNA sequencing and improved detection accuracy.

De Souza et al. [65] developed a hybrid sensor using graphene and hexagonal boron nitride with a nanopore, able to distinguish DNA bases through dipole-induced charge variations, leading to distinct current signatures. Their work demonstrated a key mechanism for DNA sensing, dependent on altering the chemical potential through a gate voltage [66], [67]. Sensitivity is closely linked to gate potential and bias voltage, as gate potential modulates the current path. Our research shows that the Z-shaped sensor requires precise gate potential and bias settings to achieve distinct signatures for the four DNA bases with high sensitivity. Optimal results were found with a dual gate biased at 2 V on each side and a fixed bias of +0.5V between electrodes. The small nanopore size of approximately 12 Å, coupled with hydrogen passivation of the silicene edges, ensures precise single-base resolution. This design outperforms earlier nanopore sensors with larger pore sizes, which struggled with base overlap and reduced accuracy. Graphene-based nanopores, as reported in Ref. [68], exhibit relatively low current values in the range of 0.1–1 $\mu$A, whereas silicene nanopores demonstrate improved performance with current values between 1–5 $\mu$A [69], attributed to its tunable bandgap and geometry. Notably, the device proposed in the present study achieves significantly higher current levels ranging from 9–30 $\mu$A, despite having a smaller channel width of only 6 nm. This enhanced performance is attributed to Z-shape geometry, which facilitates improved carrier transport through the nanopore. These results underscore the potential of modified silicene nanoribbons for high-sensitivity biosensing applications. Furthermore, the Z-shaped sensor achieves current levels in the microampere range at low bias voltages, a significant improvement over the nanoampere-scale currents of previous designs. Having a clear distinction in the presence of the different DNA signatures is a key feature in our design. This feature reduces the need for slowed DNA translocation, allowing for faster sequencing speeds without compromising accuracy. In our DNA sequencing study, transport calculations were performed for each nucleobase translocating through the silicene nanopore at orientations of 0°, 90°, and 120°. These specific orientations were chosen to account for the rotational freedom of nucleobases during translocation, since thermal fluctuations, molecular interactions, and steric effects can lead to variations in their alignment with respect to the nanopore.

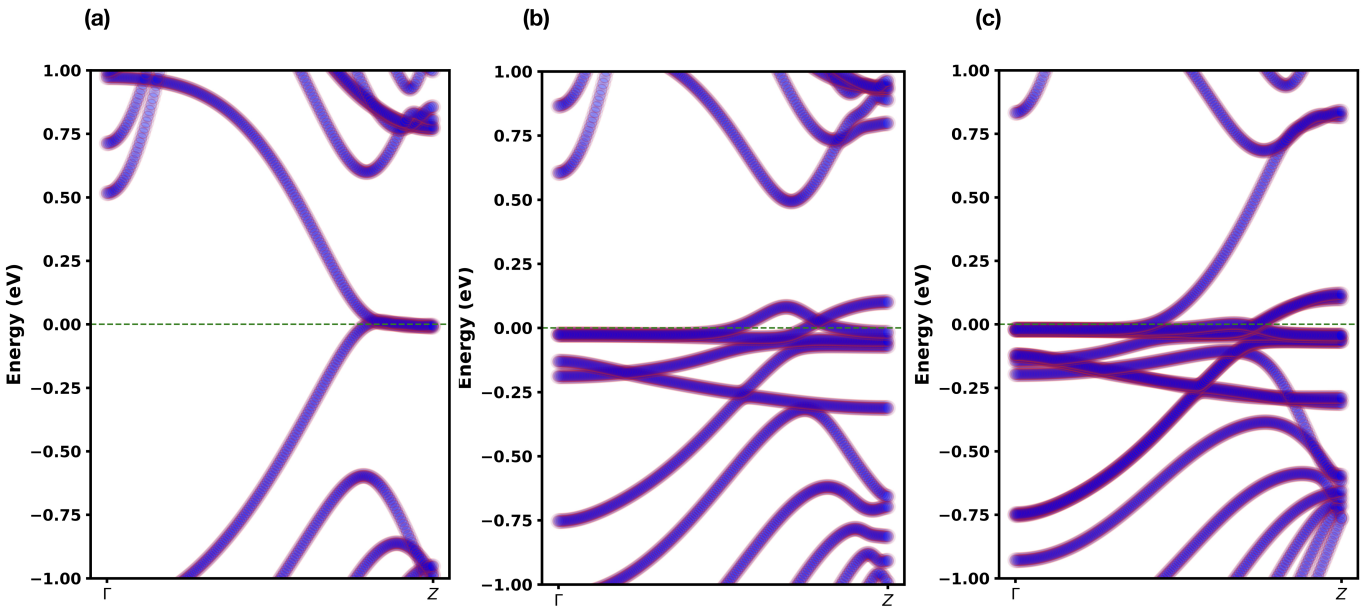



Fig. 8. Bandstructure of electrodes with different passivation (a) With all Hydrogen, (b) with one Co and another H (c) with both Co

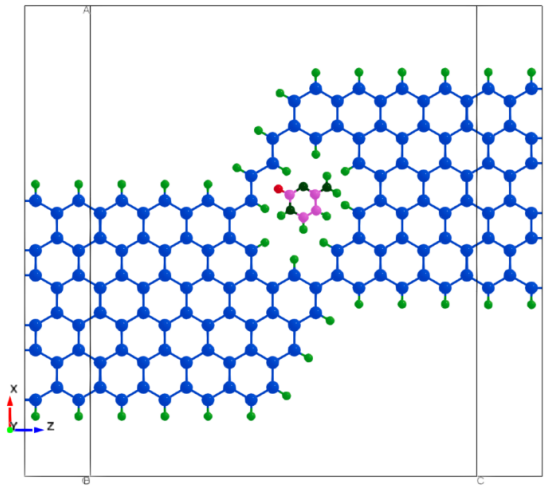


Fig. 9. (a) Z-shaped(mirror) FET silicene sensor for DNA sequencing with passivated nanopore, light green-hydrogen, blue- silicene, red- oxygen, dark green- carbon, purple-nitrogen

The calculated current spectra revealed distinct value ranges for different bases under each orientation, which not only highlights the sensitivity of silicene to molecular orientation but also enhances the robustness of base discrimination. As shown in Fig. 13, the separation of current ranges across orientations confirms that reliable identification of nucleobases is feasible even in the presence of configurational variability. To validate the reliability of our simulations in the absence of an explicit solvent environment, we performed a control calculation by introducing a single water molecule into the nanopore region without any DNA base. The resulting current exhibited a negligible change from $1.8028 \times 10^{-5}$ A (empty pore) to $1.8032 \times 10^{-5}$ A, corresponding to a difference of merely 4 nA. This minimal perturbation suggests that the presence of a water molecule does not significantly alter the charge transport characteristics of the nanopore device. Consequently, the simulations carried out for DNA bases without explicit water molecules remain robust and physically meaningful. The weak influence of water supports the assumption that the intrinsic electronic effects of DNA bases dominate the current response, validating our approach to perform base-specific transport simulations in the absence of an explicit solvent environment.

We have further calculated the device's sensitivity, although our zero-bias transmission spectra results are quite promising to distinguish the four nucleobases. However, sensing a molecule is dependent on the difference in its conductance.

The sensitivity percentage (S%) can be calculated as-

$$Sensitivity\% = \left| \frac{G - G_0}{G_0} \right|$$

where-

- $G$ is the conductance of the nanopre FET + nucleobase system,
- $G_0$ is the conductance of pristine nanopore FET at zero bias.

The results show that cytosine induces the largest change in current, followed by guanine, thymine, and adenine. Cytosine and guanine produce sensitivities of 77.37% and 70.66%, respectively, indicating strong perturbations in the transport

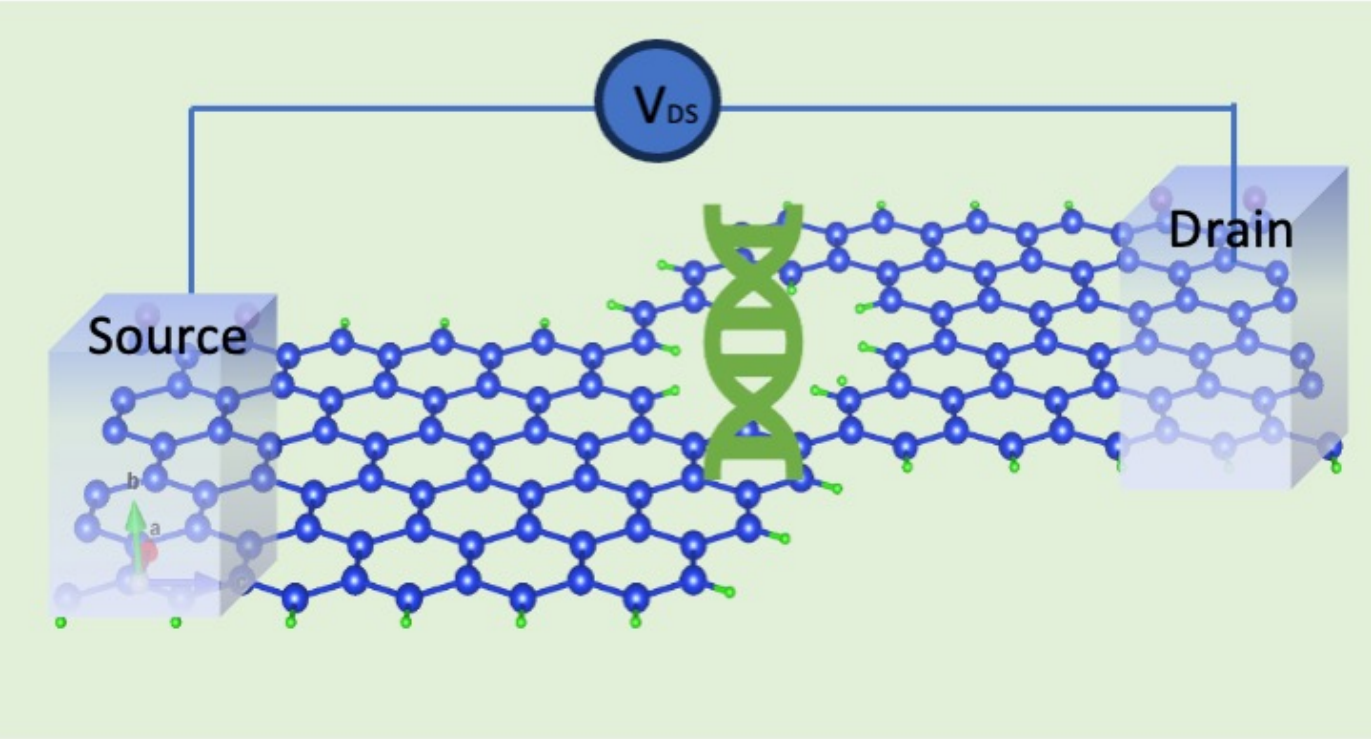



Fig. 10. 3D visual representation of DNA sequencing nanopore based field effect transistor

characteristics of the nanopore. In contrast, adenine exhibits the lowest sensitivity (7.37%), suggesting minimal interaction with the channel. These differences highlight the potential of the sensor to distinguish between DNA bases based on current signatures.

**5. Machine Learning-Assisted Sequencing of DNA Using a Silicene Nanoribbon Nanopore**

### *A. Machine Learning Methodology*

The electrical signals generated during DNA translocation through solid-state nanopores often exhibit significant overlap due to thermal noise, molecular conformational fluctuations, and device-induced variability, making direct base identification challenging. As shown in Fig. 12, the raw current responses associated with different nucleobases are not always sharply separated. This limited distinguishability originates from the intrinsic overlap in the corresponding transmission spectra, which leads to partially overlapping current distributions even under identical bias conditions. Such overlap significantly complicates direct threshold-based base identification and provides a strong motivation for incorporating machine-learning techniques to extract subtle, high-dimensional patterns from the transport data. To address this fundamental limitation, machine-learning techniques have recently emerged as powerful tools for extracting subtle and discriminative features from quantum transport data [70]–[74].

Motivated by these studies, we adopt a similar feature-engineering strategy for constructing the machine-learning dataset; however, the learning model itself is independently developed and optimized for the current signatures obtained from our Z-shaped silicene nanoribbon nanopore device. Unlike previous works that primarily focused on graphene and related materials, the present framework is specifically tailored to the distinct electronic response of silicene. This combined device–algorithm approach enables robust and automated DNA base identification even in the presence of strongly overlapping signal distributions. The overall ML workflow is illustrated schematically in Fig. 14.

The transmission spectra obtained from DFT-NEGF calculations were first preprocessed by selecting an optimized energy window around the Fermi level, where maximal separation between nucleotide signatures was observed. From each transmission profile, six physically motivated features were extracted- $E$, $T$, $T/T_{\max}$, $T/T_{\min}$, $T/T_{\text{avg}}$, and $T/T_{\text{hm}}$, where $T_{\max}$, $T_{\min}$, $T_{\text{avg}}$, and $T_{\text{hm}}$ represent the maximum, minimum, arithmetic mean, and harmonic mean of the transmission spectrum, respectively. These normalized descriptors amplify subtle variations in electrode-molecule coupling and significantly enhance nucleotide distinguishability.

The resulting dataset was randomly divided into training (80%) and testing (20%) subsets while preserving class balance. Several ML classifiers were evaluated, including k-

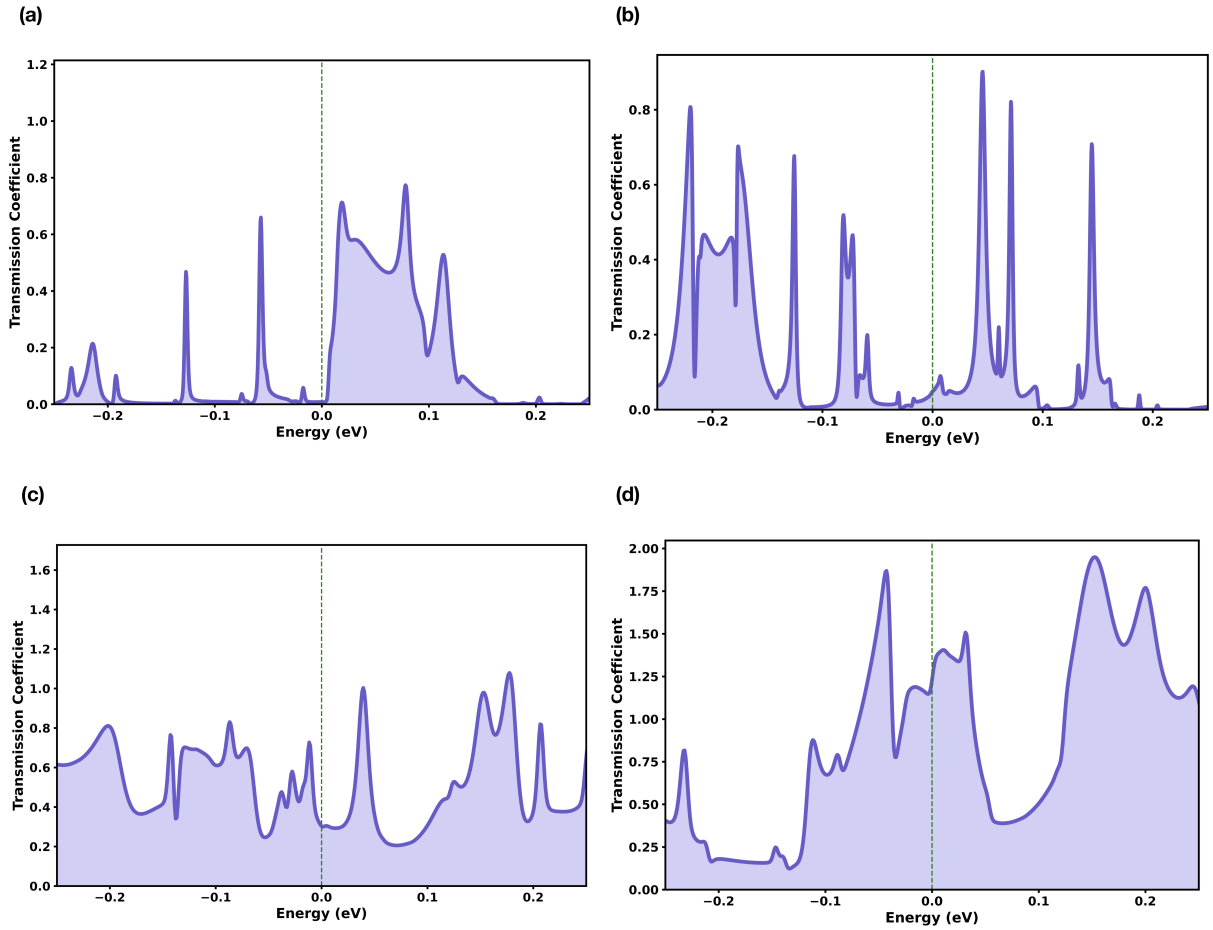



Fig. 11. Transmission spectrum of (a) guanine (b) cytosine (c) adenine (d) thymine

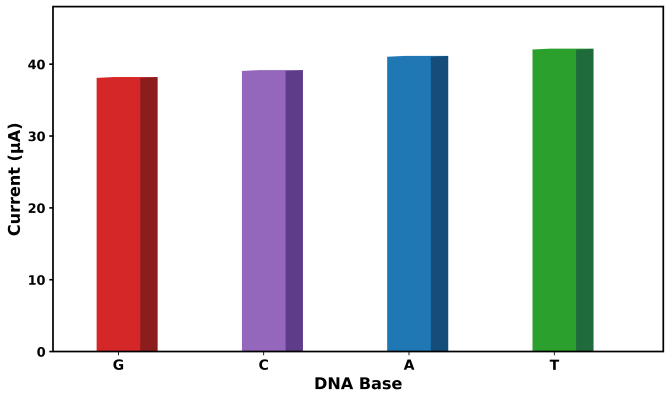



Fig. 12. Current in microamperes for each DNA base molecule with all hydrogen passivation

nearest neighbors (KNN), logistic regression, random forest, naive Bayes, and support vector machines (SVM) as implemented in Scikit-learn package 0.23.1 [75]. Among them, random forest consistently exhibited superior performance. Hyperparameter optimization was carried out using GridSearchCV with stratified five-fold cross-validation over a broad range of the regularization parameter $C$ and kernel width $\gamma$.

### *B. . Model Evaluation and Performance*

Model performance was assessed using accuracy, precision, recall, and F1-score, defined as

$$\text{Accuracy} = \frac{TP + TN}{TP + TN + FP + FN}, \tag{4}$$

$$\text{Precision} = \frac{TP}{TP + FP}, \tag{5}$$

$$\text{Recall} = \frac{TP}{TP + FN}, \tag{6}$$

$$\text{F1-score} = \frac{2 \times \text{Precision} \times \text{Recall}}{\text{Precision} + \text{Recall}}. \tag{7}$$

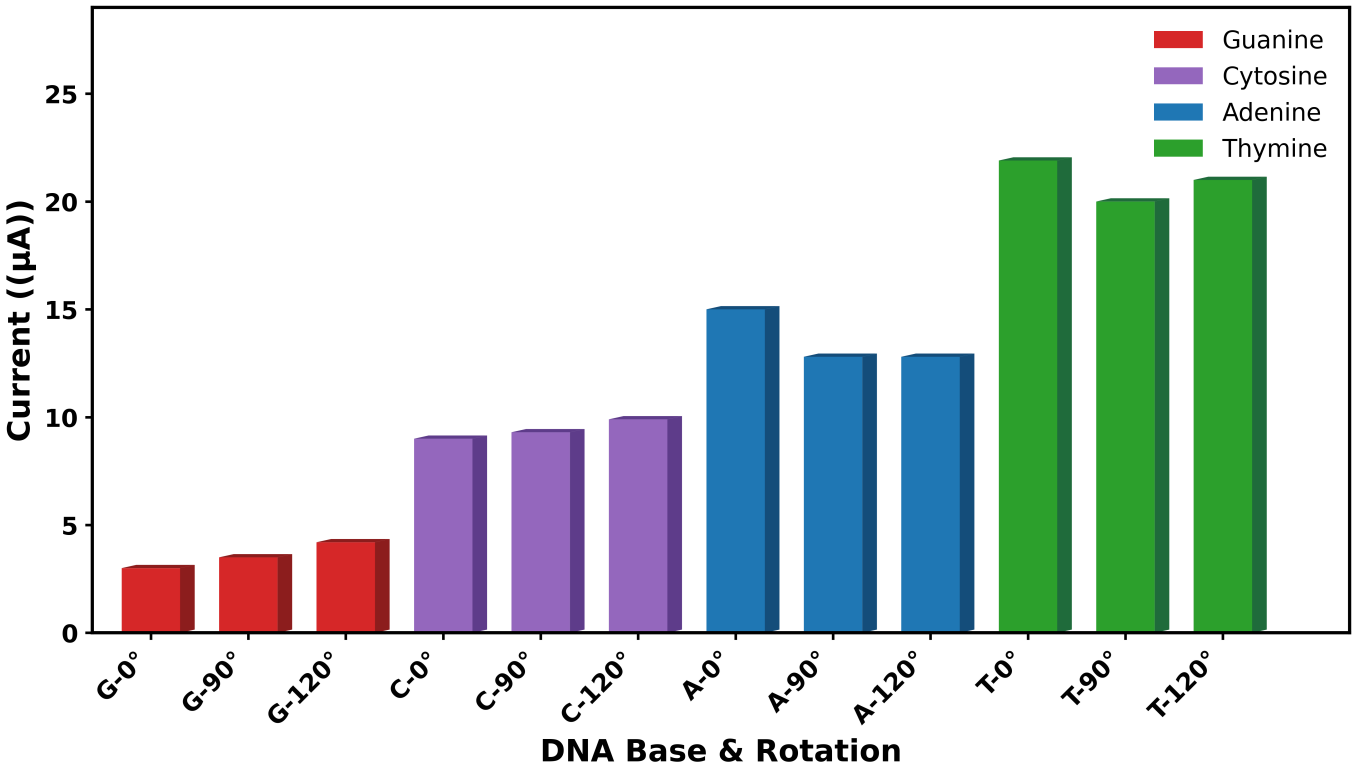



Fig. 13. Current in microamperes for each DNA base molecule with additional cobalt functionalization at leads with. All the bases were translocated at angles 0,90,120 degrees with respect to horizontal silicene nanopore( shown in Fig. 10)

The optimized random forest model achieved a classification accuracy exceeding 99.2% for the simultaneous identification of the four natural nucleotides (A, T, C, and G). The corresponding confusion matrix is presented in Fig. 17. The matrix demonstrates strong diagonal dominance, indicating a high proportion of correct classifications for each nucleotide. Only a small number of misclassification events are observed, primarily between chemically similar bases, confirming that the model effectively captures the subtle differences in the quantum transport signatures.

The class-wise precision, recall, and F1-scores extracted from the confusion matrix further confirm the robustness of the classifier, with all metrics exceeding 90% for each nucleotide. This highlights the model's ability to maintain both high sensitivity and specificity in base calling.

To evaluate model generalization, we further performed stratified 5-fold cross-validation. The average cross-validated accuracy closely matched the independent test accuracy, indicating negligible overfitting and strong predictive reliability.

Table II compares the performance of multiple machine learning models. Among all tested classifiers, the random forest model achieves the highest predictive accuracy (99.2%), precision, recall, F1-score, and cross-validation accuracy, demonstrating superior generalization and robustness. While the Random Forest model achieves the highest and most stable performance, reaching a test accuracy of 99.2% together with precision, recall, and F1-score of 0.99 and a cross-validation accuracy of 99.58% (CV std = 0.0037), the SVM with RBF kernel also demonstrates strong classification capability, yielding an accuracy of 97.92%. The corresponding confusion matrix (Fig. X) further confirms this behavior, showing high true-positive rates across all nucleobase classes with only minor misclassification near class boundaries, arising from partial overlap in the underlying transport features. In contrast, Logistic Regression and KNN exhibit only moderate performance (accuracies of 77.9% and 81.7%, respectively), indicating their limited ability to capture the nonlinear relationships inherent in the transport data. The Naive Bayes classifier performs poorly with an accuracy of only 45.0%, reflecting a strong violation of its conditional independence assumptions for this dataset. Cross-validation metrics are not reported for the Naive Bayes classifier because the strong correlation among the transport features violates its conditional independence assumption, leading to unstable and non-informative performance estimates across validation folds. Collectively, these results highlight the necessity of nonlinear, ensemble-based learning strategies for reliable nucleobase discrimination in nanoscale sequencing devices.

These results confirm that the nonlinear ensemble-based random forest classifier is most suitable for the present quantum-transport-based DNA sequencing task.

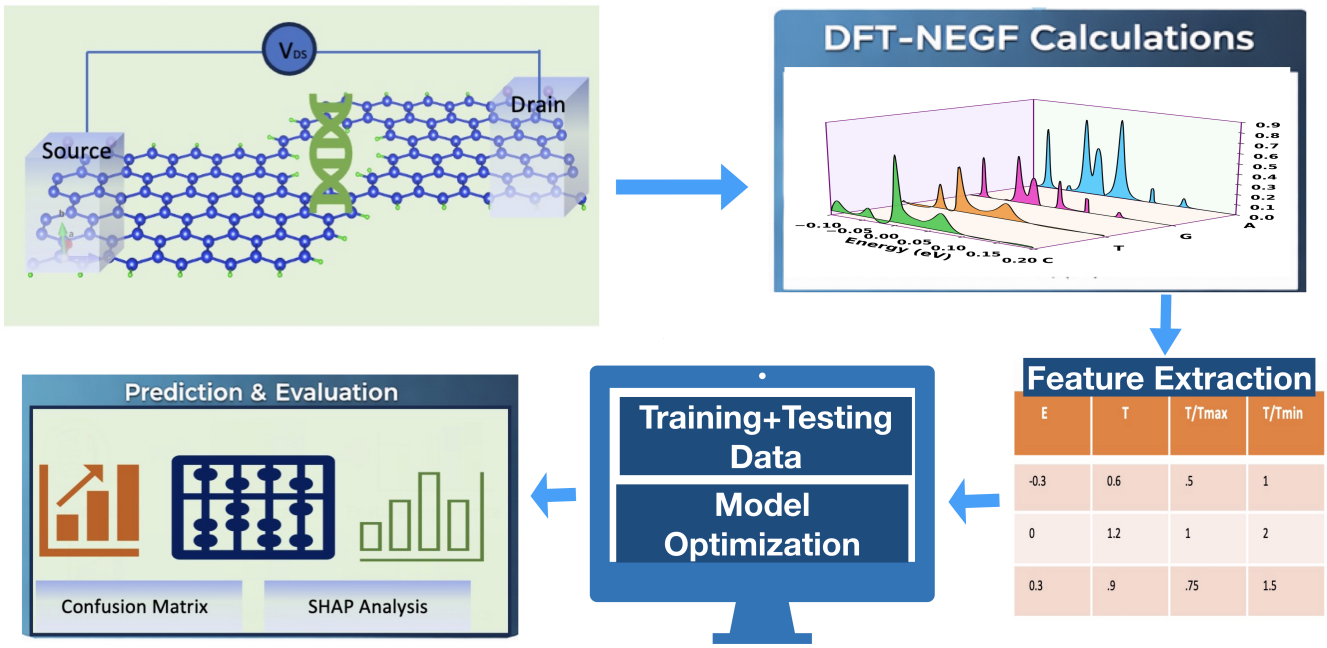



Fig. 14. Machine learning workflow for classifying DNA nucleotides

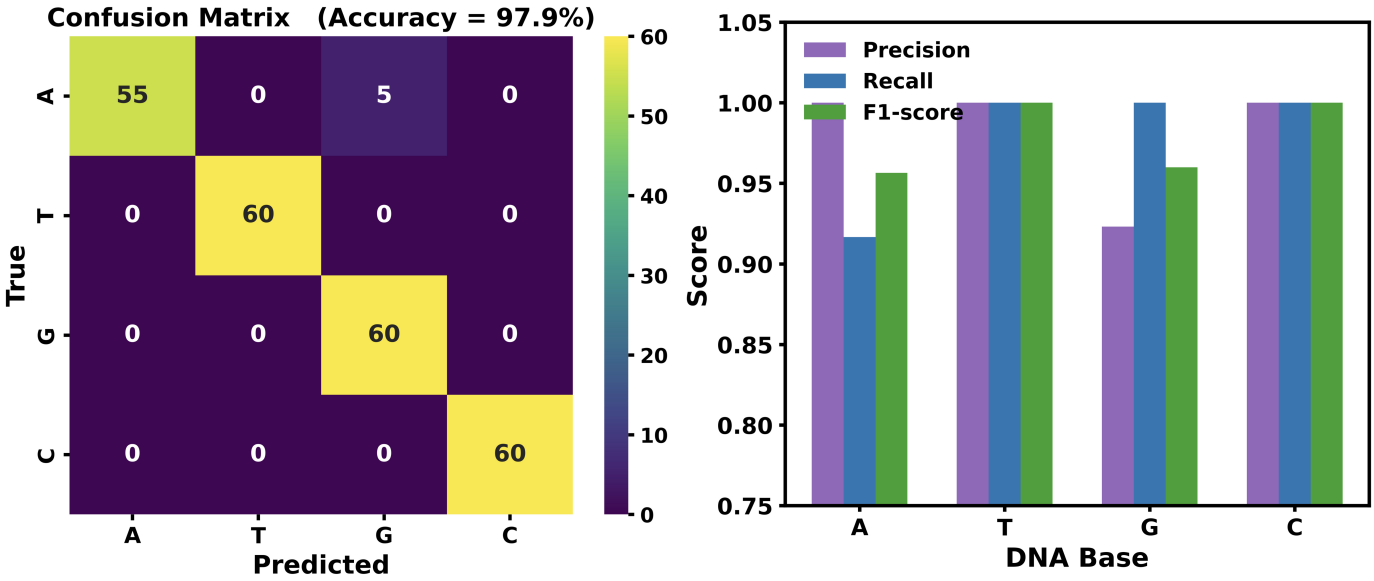



Fig. 15. SVC (RBF) (a) confusion matrix (b) classification report for classification of nucleotides (A, T, C, G)

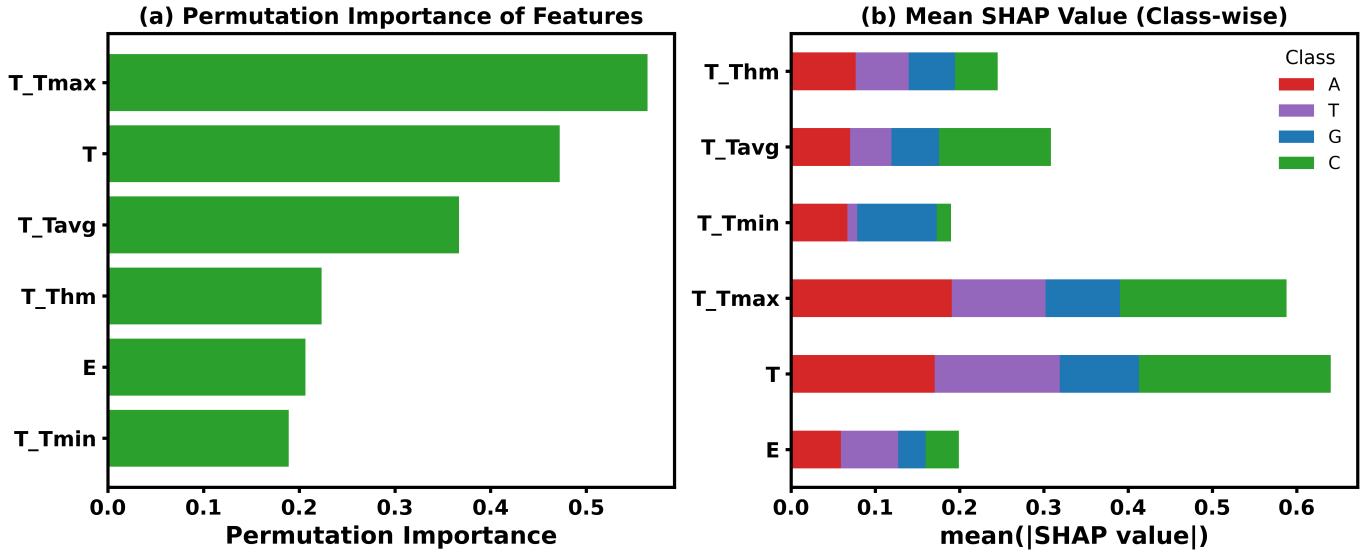



Fig. 16. SVC (RBF) (a) permutation feature importance bar plots and (b) SHAP analysis for classification of nucleotides

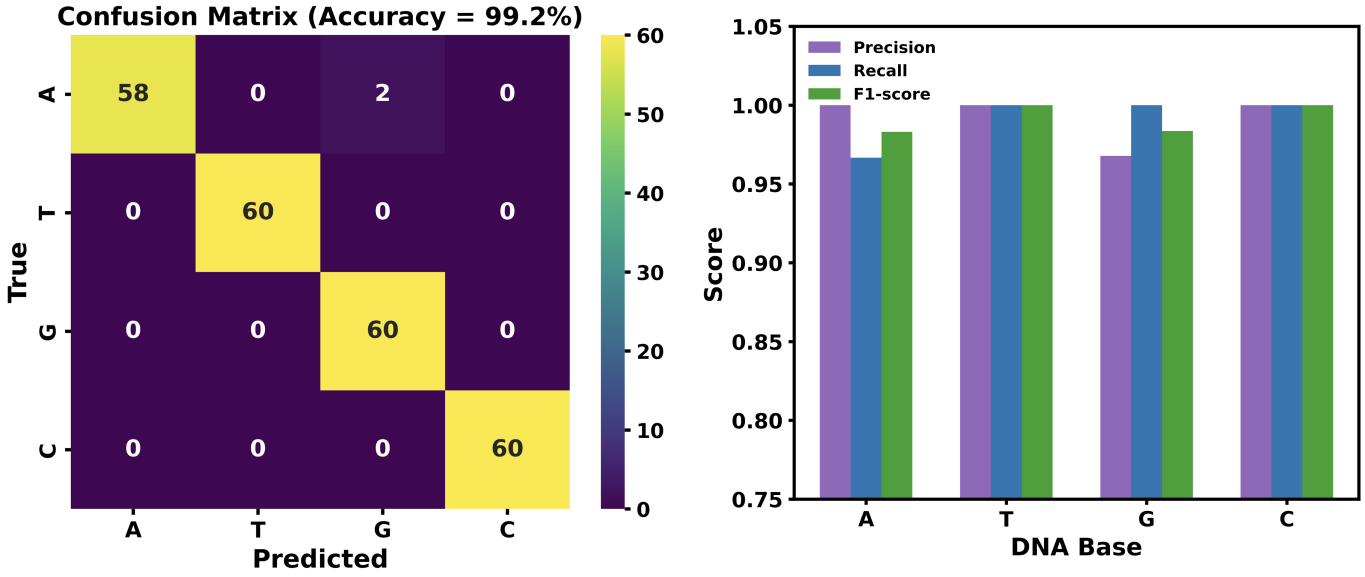



Fig. 17. Random forest (a) confusion matrix (b) classification report for classification of nucleotides (A, T, C, G)

### C. *Interpretability - Feature Importance and SHAP Analysis*

To interpret the ML decision-making process, we analyzed permutation feature importance and SHapley Additive exPlanations (SHAP) values. The permutation analysis revealed that the normalized transmission features $T/T_{\text{hm}}$, $T/T_{\text{min}}$, $T/T_{\text{avg}}$, and $T/T_{\text{max}}$ dominate the model predictions, whereas the raw descriptors $E$ and $T$ exhibit comparatively lower influence.

SHAP analysis (Fig. 16,18) provided deeper insight into local feature contributions for individual nucleotide predictions. Features associated with strong electrode-molecule coupling and transmission fluctuations were found to play a decisive role in distinguishing chemically similar nucleobases. The consistent agreement between SHAP and permutation results confirms the physical relevance of the selected descriptors.

## 6. Conclusion

This study advances nanopore-based DNA sequencing by exploiting the exceptional electronic properties of silicene together with the novel geometry of a Z-shaped nanoribbon FET. Using first-principles DFT+NEGF transport simulations, we demonstrate that individual DNA bases, under multiple ro-

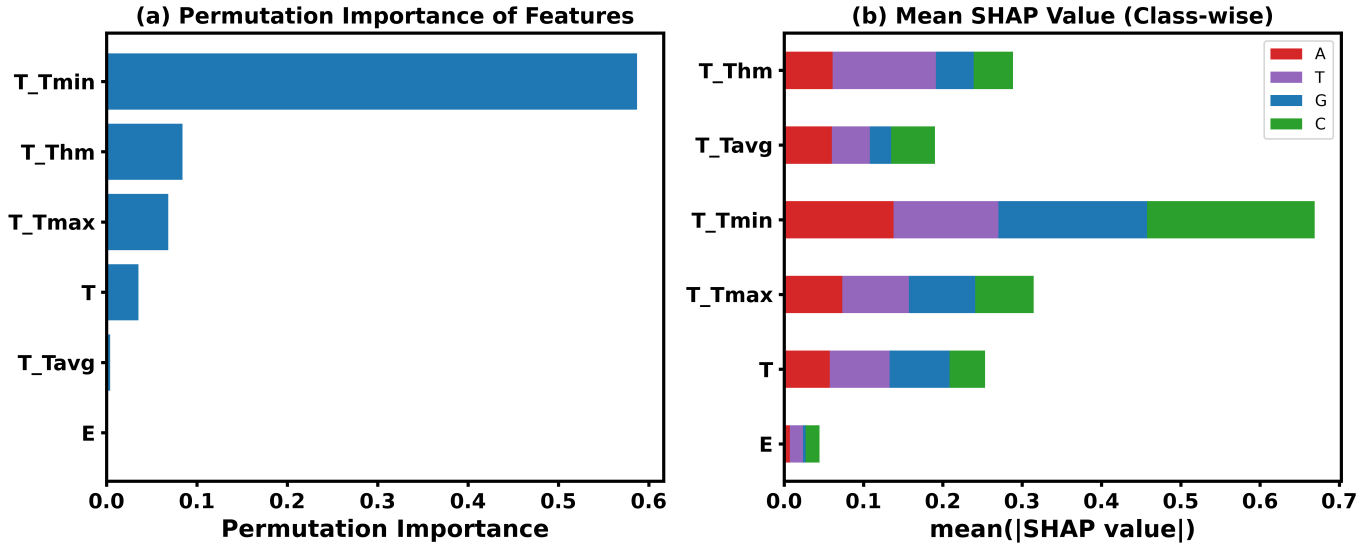



Fig. 18. Random forest (a) permutation feature importance bar plots and (b) SHAP analysis for classification of nucleotides

TABLE II
PERFORMANCE COMPARISON OF DIFFERENT MACHINE LEARNING MODELS FOR DNA BASE CLASSIFICATION.

| Model | Test Accuracy | Precision | Recall | F1-score | CV Accuracy | CV Std |
|---|---|---|---|---|---|---|
| SVC (RBF) | 0.9792 | 0.9808 | 0.9792 | 0.9791 | 0.9842 | 0.0085 |
| Logistic Regression | 0.7792 | 0.8116 | 0.7792 | 0.7755 | 0.8208 | 0.0293 |
| Random Forest | **0.992** | **0.9900** | **0.9900** | **0.9900** | **0.9958** | **0.0037** |
| KNN | 0.8167 | 0.8169 | 0.8167 | 0.8152 | 0.8500 | 0.0280 |
| Naive Bayes | 0.4500 | 0.5037 | 0.4500 | 0.4107 | - | - |

tational orientations, generate distinct current signatures when translocating through a silicene nanopore. This orientation-aware analysis significantly enhances base selectivity and robustness, addressing key limitations of existing nanopore technologies. These findings highlight asymmetric passivation of electrodes as an effective device-engineering strategy to enhance the performance of silicene-based bioelectronic sequencing devices.

The proposed sensor achieves high sensitivity and resolution while offering a scalable, low-power platform suitable for next-generation sequencing applications. Moreover, the integration of machine learning with the silicene nanoribbon nanopore device effectively resolves the inherent overlap in quantum transport signals, enabling rapid, accurate, and automated nucleotide identification on a single solid-state platform. From a practical perspective, the proposed ML framework can be implemented directly within the electronic readout circuitry of a nanopore sequencing chip, where the measured current–voltage signals are streamed in real time to an embedded processor for on-chip classification. Such integration would enable immediate base identification without the need for extensive post-processing, thereby significantly reducing sequencing latency and power consumption. In a clinical setting, this capability could facilitate rapid point-of-care genetic screening for disease diagnostics, pathogen detection, and personalized treatment planning. By enabling fast, low-cost, and portable sequencing platforms, the combined silicene–ML approach holds strong potential for widespread deployment in hospitals, diagnostic laboratories, and remote healthcare environments.

These results establish a unified DFT–NEGF–ML framework and lay a strong foundation for the design of ultrathin, label-free biosensors with direct relevance to real-time genetic screening and precision medicine. With further experimental validation and integration into portable diagnostic systems, this approach has the potential to accelerate the development of affordable, accurate, and accessible DNA sequencing technologies, transforming personalized healthcare and genomics.

## REFERENCES

[1] Richard M Martin. *Electronic Structure: Basic Theory and Practical Methods*. Cambridge University Press, 2004.
[2] Walter Kohn. Nobel lecture: Electronic structure of matter—wave functions and density functionals. *Reviews of Modern Physics*, 71(5):1253–1266, 1999.
[3] Kristian S Thygesen. Calculating electron transport using dft and negf: The art of the possible. *Physical Chemistry Chemical Physics*, 19(35):23128–23136, 2017.
[4] S. Das et al. First-principles investigation of materials for biosensing applications. *Biosensors and Bioelectronics*, 164:112276, 2020.
[5] Mads Brandbyge, José-Luis Mozos, Pablo Ordejón, Jeremy Taylor, and Kurt Stokbro. Density-functional method for nonequilibrium electron transport. *Physical Review B*, 65(16):165401, 2002.
[6] Troels Markussen, Robert Stadler, and Kristian S Thygesen. The relation between structure and quantum interference in single molecule junctions. *Nano Letters*, 10(10):4260–4265, 2010.

[7] Fang Chen, Joshua Hihath, Zhenyu Huang, Xuefeng Li, and Nongjian Tao. Measurement of single-molecule conductance. *Annual Review of Physical Chemistry*, 58:535–564, 2007.

[8] Arieh Warshel. Multiscale modeling of biological functions: From enzymes to molecular machines (nobel lecture). *Angewandte Chemie International Edition*, 53(38):10020–10031, 2014.

[9] Sheng Gao et al. Theoretical insights into electrochemical $co_2$ reduction over single-atom catalysts: A dft study. *ChemSusChem*, 13(4):1009–1017, 2020.

[10] Kamalika Saha and Marija Drndić. Dna base discrimination using a graphene nanopore: A first-principles study. *Nano Letters*, 14(1):118–123, 2014.

[11] Yifan Zhang and Feng Wang. Dft+negf simulations of dna sequencing using 2d materials. *The Journal of Physical Chemistry C*, 125(42):23645–23652, 2021.

[12] H. P. J. Buermans and J. T. den Dunnen. Next generation sequencing technology: Advances and applications. *Biochimica et Biophysica Acta (BBA) - Molecular Basis of Disease*, 1842(10):1932–1941, 2014.

[13] Y. Feng, Y. Zhang, C. Ying, D. Wang, and C. Du. Nanopore-based fourth-generation dna sequencing technology. *Genomics, Proteomics & Bioinformatics*, 13(1):4–16, 2015.

[14] L. M. Smith, J. Z. Sanders, R. J. Kaiser, and et al. Fluorescence detection in automated dna sequence analysis. *Nature*, 321(6071):674–679, 1986.

[15] D. R. Bentley. Whole-genome re-sequencing. *Current Opinion in Genetics & Development*, 18(3):226–232, 2008.

[16] E. R. Mardis. Dna sequencing technologies: 2006–2016. *Nature Protocols*, 12(1):365–368, 2017.

[17] D. Branton, D. W. Deamer, A. Marziali, and et al. The potential and challenges of nanopore sequencing. *Nature Biotechnology*, 26(10):1146–1153, 2008.

[18] J. Eid, A. Fehr, J. Gray, and et al. Real-time dna sequencing from single polymerase molecules. *Science*, 323(5910):133–138, 2009.

[19] H. Bayley. Sequencing single molecules of dna. *Journal of Molecular Biology*, 428(7):1–21, 2015.

[20] D. Stoddart, A. J. Heron, E. Mikhailova, and et al. Single-nucleotide discrimination in immobilized dna oligonucleotides with a biological nanopore. *Proceedings of the National Academy of Sciences*, 106(19):7702–7707, 2009.

[21] J. J. Kasianowicz, E. Brandin, D. Branton, and D. W. Deamer. Characterization of individual polynucleotide molecules using a membrane channel. *Proceedings of the National Academy of Sciences*, 93(24):13770–13773, 1996.

[22] E. A. Manrao, I. M. Derrington, A. H. Laszlo, K. W. Langford, M. M. Hopper, and J. H. Gundlach. Reading dna at single-nucleotide resolution with a mutant mycobacterium smegmatis porin. *Nature Biotechnology*, 30(4):349–354, 2012.

[23] C. Dekker. Solid-state nanopores. *Nature Nanotechnology*, 2(4):209–215, 2007.

[24] B. N. Miles, A. P. Ivanov, K. A. Wilson, and et al. Single-molecule sensing with solid-state nanopores: Novel materials, methods, and applications. *Chemical Society Reviews*, 42(1):15–28, 2013.

[25] B. M. Venkatesan and R. Bashir. Nanopore sensors for nucleic acid analysis. *Nature Nanotechnology*, 6(11):615–624, 2011.

[26] S. Garaj, W. Hubbard, A. Reina, and et al. Graphene as a subnanometre trans-electrode membrane. *Nature*, 467(7312):190–193, 2010.

[27] C. A. Merchant, K. Healy, M. Wanunu, and et al. Dna translocation through graphene nanopores. *Nano Letters*, 10(8):2915–2921, 2010.

[28] R. M. Smeets, U. F. Keyser, N. H. Dekker, and et al. Salt dependence of ion transport and dna translocation through solid-state nanopores. *Nano Letters*, 8(5):1346–1350, 2008.

[29] H. W. Postma. Rapid sequencing of individual dna molecules in graphene nanogaps. *Nano Letters*, 10(2):420–425, 2010.

[30] P. Vogt, P. De Padova, C. Quaresima, and et al. Silicene: Compelling experimental evidence for graphenelike two-dimensional silicon. *Physical Review Letters*, 108(15):155501, 2012.

[31] A. Molle and C. Grazianetti. Xenes – 2d synthetic materials beyond graphene. In *Xenes – 2D Synthetic Materials Beyond Graphene*. Woodhead Publishing, Sawston, UK, 2022.

[32] C. Grazianetti and C. Martella. The rise of the xenes: From the synthesis to the integration processes for electronics and photonics. *Materials*, 14(15):4170, 2021.

[33] N. R. Glavin. Emerging applications of elemental 2d materials. *Advanced Materials*, 32(7):1904302, 2020.

[34] A. J. Mannix, B. Kiraly, M. C. Hersam, and N. P. Guisinger. Synthesis and chemistry of elemental 2d materials. *Nature Reviews Chemistry*, 1(2):0014, 2017.

[35] M. E. Dávila and G. Le Lay. Silicene: Genesis, remarkable discoveries, and legacy. *Materials Today Advances*, 16:100312, 2022.

[36] C.-C. Liu, W. Feng, and Y. Yao. Quantum spin hall effect in silicene and two-dimensional germanium. *Physical Review Letters*, 107(7):076802, 2011.

[37] L. Matthes, O. Pulci, and F. Bechstedt. Massive dirac quasiparticles in the optical absorbance of graphene, silicene, germanene, and tinene. *Journal of Physics: Condensed Matter*, 25(39):395305, 2013.

[38] M. Houssa. Theoretical aspects of graphene-like group iv semiconductors. *Applied Surface Science*, 291:98–103, 2014.

[39] X. Li, J. T. Mullen, Z. Jin, K. M. Borysenko, M. Buongiorno Nardelli, and K. W. Kim. Intrinsic electrical transport properties of monolayer silicene and $MoS_2$ from first principles. *Physical Review B*, 87(11):115418, 2013.

[40] C. Grazianetti and A. Molle. Engineering epitaxial silicene on functional substrates for nanotechnology. *Research*, 2019:1–8, 2019.

[41] C. Grazianetti. Optical conductivity of two-dimensional silicon: Evidence of dirac electrodynamics. *Nano Letters*, 18(11):7124–7132, 2018.

[42] Z. I. Alferov. The double heterostructure concept and its applications in physics, electronics, and technology. *Reviews of Modern Physics*, 73(3):767–782, 2001.

[43] Y. Kim. Remote epitaxy through graphene enables two-dimensional material-based layer transfer. *Nature*, 544(7650):340–343, 2017.

[44] C. Grazianetti, A. Molle, and C. Martella. Silicene applications in nanotechnology: From transistors to bendable membranes. *IEEE Transactions on Materials for Electron Devices*, 1:1–10, 2024.

[45] D. S. Dhungana, C. Grazianetti, C. Martella, S. Achilli, G. Fratesi, and A. Molle. Two-dimensional silicene–stanene heterostructures by epitaxy. *Advanced Functional Materials*, 31:2102797, 2021.

[46] S. Achilli. Crystal phase engineering of silicene by sn-modified Ag(111). *Nanoscale*, 15(26):11005–11012, 2023.

[47] D. S. Dhungana, C. Massetti, C. Martella, C. Grazianetti, and A. Molle. All-around encapsulation of silicene. *Nanoscale Horizons*, 8(10):1428–1434, 2023.

[48] E. Cinquanta. Optical response and ultrafast carrier dynamics of the silicene–silver interface. *Physical Review B*, 92(16):165427, 2015.

[49] E. Cinquanta. Getting through the nature of silicene: An $sp^2$–$sp^3$ two-dimensional silicon nanosheet. *Journal of Physical Chemistry C*, 117(32):16719–16724, 2013.

[50] A. Molle. Stability and universal encapsulation of epitaxial xenes. *Faraday Discussions*, 227:171–183, 2021.

[51] V. Ritter, J. Genser, D. Nazzari, O. Bethge, E. Bertagnolli, and A. Lugstein. Silicene passivation by few-layer graphene. *ACS Applied Materials & Interfaces*, 11(13):12745–12751, 2019.

[52] H. Wang, C. Wang, Y. Zhang, Z. Wang, Y. Zhu, Y. Wang, X. Hong, H. Zhang, N. Fan, and M. Qiu. Recent advances in xenes based fet for biosensing applications. *Advanced Science*, 12(21):2500752, 2025.

[53] H. Sadeghi. Electrical transport model of silicene as a channel of field effect transistor. *Journal of Nanoscience and Nanotechnology*, 14(6):4178–4184, 2014.

[54] L. Tao, E. Cinquanta, D. Chiappe, C. Grazianetti, M. Fanciulli, M. Dubey, A. Molle, and D. Akinwande. Silicene field-effect transistors operating at room temperature. *Nature Nanotechnology*, 10(3):227–231, 2015.

[55] E. Kozma, C. Martella, A. E. Andicsová, S. Gharedaghi, A. Lamperti, C. Massetti, A. Opálek, C. Grazianetti, F. Galeotti, and A. Molle. Vacuum–nitrogen assisted (vans) topotactical deintercalation for extremely fast production of functionalized silicene nanosheets. *Small*, 21(7):2406088, 2025.

[56] A. Molle, C. Grazianetti, L. Tao, D. Taneja, M. H. Alam, and D. Akinwande. Silicene, silicene derivatives, and their device applications. *Chemical Society Reviews*, 47(16):6370–6387, 2018.

[57] H. Sadeghi, S. Bailey, and C. J. Lambert. Silicene-based dna nucleobase sensing. *Applied Physics Letters*, 104(10):103104, 2014.

[58] Surjit Bhai and Bishwajit Ganguly. 2d silicene nanosheets for the detection of dna nucleobases for genetic biomarker: a DFT study. *Structural Chemistry*, 35(1):25–37, 2024.

[59] Rodrigo G. Amorim and Ralph H. Scheicher. Silicene as a new potential DNA sequencing device. *Nanotechnology*, 26(15):154002, 2015.

[60] R. Chandiramouli and V. Nagarajan. Silicene nanosheet device with nanopore to identify the nucleobases – a first-principles perspective. *Chemical Physics Letters*, 730:70–75, 2019.
[61] NanoAcademic Technologies Inc. Nanoacademic technologies inc. http://www.nanoacademic.ca/.
[62] S. Datta and B. Das. Electronic analog of the electro-optic modulator. *Applied Physics Letters*, 56(7):665–467, 1990.
[63] M. Büttiker, Y. Imry, R. Landauer, and S. Pinhas. Generalized many-channel conductance formula with application to small rings. *Physical Review B*, 31(10):6207–6215, 1985.
[64] Manabu Sugimoto, Yuta Kato, Kentaro Ishida, Changbae Hyun, Jiali Li, and Toshiyuki Mitsui. Dna motion induced by electrokinetic flow near an au coated nanopore surface as voltage controlled gate. *Nanotechnology*, 26(6):065502, 2015.
[65] F. A. de Souza, R. G. Amorim, W. L. Scopel, and R. H. Scheicher. Electrical detection of nucleotides via nanopores in a hybrid graphene/h-bn sheet. *Nanoscale*, 9(6):2207–2212, 2017.
[66] J. Prasongkit, E. de Freitas Martins, F. A. de Souza, W. L. Scopel, R. G. Amorim, V. Amornkitbamrung, A. R. Rocha, and R. H. Scheicher. Topological line defects around graphene nanopores for dna sequencing. *The Journal of Physical Chemistry C*, 122(13):7094–7099, 2018.
[67] F. Schedin, A. K. Geim, S. V. Morozov, E. W. Hill, P. Blake, M. I. Katsnelson, and K. S. Novoselov. Detection of individual gas molecules adsorbed on graphene. *Nature Materials*, 6:652–655, 2007.
[68] A. Wasfi, F. Awwad, and A. I. Ayesh. Dna sequencing via z-shaped graphene nano ribbon field effect transistor decorated with nanoparticles using first-principle transport simulations. *New Journal of Physics*, 22(6):063004, 2020.
[69] R. Chandiramouli and V. Nagarajan. Silicene nanosheet device with nanopore to identify the nucleobases–a first-principles perspective. *Chemical Physics Letters*, 730:70–75, 2019.
[70] M. Taniguchi, H. Takei, K. Tomiyasu, O. Sakamoto, and N. Naono. Sensing the performance of artificially intelligent nanopores developed by integrating solid-state nanopores with machine learning methods. *The Journal of Physical Chemistry C*, 126(29):12197–12209, 2022.
[71] N. Meyer, J.-M. Janot, M. Lepoitevin, M. Smietana, J.-J. Vasseur, J. Torrent, and S. Balme. Machine learning to improve the sensing of biomolecules by conical track-etched nanopore. *Biosensors*, 10(10):140, 2020.
[72] M. K. Jena, D. Roy, S. Mittal, and B. Pathak. Artificially intelligent nanogap for rapid dna sequencing: A machine learning aided quantum tunneling approach. *ACS Materials Letters*, 5(9):2488–2498, 2023.
[73] R. L. Kumawat, M. K. Jena, S. Mittal, and B. Pathak. Advancement of next–generation dna sequencing through ionic blockade and transverse tunneling current methods. *Small*, 20(36):2401112, 2024.
[74] D. Maurya, S. Mittal, M. K. Jena, and B. Pathak. Machine learning-driven quantum sequencing of natural and chemically modified dna. *ACS Applied Materials & Interfaces*, 17(14):20778–20789, 2025.
[75] F. Pedregosa, G. Varoquaux, A. Gramfort, V. Michel, B. Thirion, O. Grisel, M. Blondel, P. Prettenhofer, R. Weiss, V. Dubourg, and J. Vanderplas. Scikit-learn: Machine learning in python. *Journal of Machine Learning Research*, 12:2825–2830, 2011.

## Statements and Declarations

### *Funding*

The authors declare that no funds, grants, or other support were received during the preparation of this manuscript.

### *Competing Interests*

The authors have no relevant financial or non-financial interests to disclose.

### *Author Contributions*

Ashutosh contributed to the conceptualization, theoretical modeling, quantum transport calculations, data analysis, and manuscript preparation. Abhishek helped in the the review and analysis of the results. Prof. Arti Kashyap supervised the research, provided critical insights, and reviewed the manuscript. All authors read and approved the final manuscript.

### *Data Availability*

The data that support the findings of this study are available from the corresponding author, Prof. Arti Kashyap, upon reasonable request.

### *Corresponding Author*

Correspondence to Prof. Arti Kashyap.